Friction and inertia of a vortex in an underdamped Josephson array

U. Geigenmüller, C.J. Lobb, and C.B. Whan
Department of Physics, Center for Superconductivity Research, University of Maryland, College Park, Maryland 20740
(Received 11 May 1992)

We study the motion of massive vortices in Josephson-junction arrays by numerically solving the equations of motion for square lattices of resistively and capacitively shunted Josephson junctions. We find that the viscous drag force on a vortex, which varies as the inverse of the junction resistance for low-mass vortices, becomes independent of the junction resistance as the vortex mass increases. We present a semiquantitative model that explains this unusual behavior. As a consequence of the excess drag, ballistic vortex motion should only be observed for a limited range of parameter values, in agreement with the recent experiment of Van der Zant *et al.* [Europhys. Lett. **18**, 343 (1992)].

I. INTRODUCTION

Vortices in the phase configuration of an array of Josephson junctions dominate its dynamic properties for bias currents I_a small compared to the junction critical current I_c. Above a threshold of $I_a \approx 0.1 I_c$ (Ref. 1) the bias current causes the vortices to move. This implies that the Josephson phases change in time, voltages across the junctions appear, and currents flow through the resistors R shunting them. The accompanying energy dissipation amounts to a frictional force on the vortices, limiting their velocities.

Since the junctions also have a capacitance C, voltages imply the storage of electrostatic energy as well. This energy storage occurs simultaneously with vortex motion, and it has been interpreted[2–5] as the kinetic energy of the vortices, which therefore also should have a mass m. Simple estimates[4,5] agree with the result of a more elaborate theory[2,3] and give $m \approx (\hbar/2e)^2(2\pi/a)^2 C/2$, where a is the lattice constant, and $-e$ is the electronic charge.

Accepting the concept of a massive vortex it is conceivable that, for sufficiently high mass and low damping, *ballistic* vortex motion becomes possible: a vortex, once accelerated by an externally applied current I_a, should travel for many lattice constants after I_a has been switched off, until eventually it is brought to rest by the remaining friction.

Last year, an important experiment by Van der Zant *et al.*[6] indicated the existence of ballistic vortices. Shortly afterward, however, Bobbert[7] conducted the first systematic numerical study of vortex motion in underdamped Josephson arrays, and found a greatly enhanced friction as compared to the theoretical predictions. He could not detect ballistic vortex motion.

Motivated by this discrepancy, we also performed a numerical investigation of vortex motion. We avoided approximating the sinusoidal Josephson potential by a piecewise linear function as done in Ref. 7. The calculation is very straightforward and described in Sec. II. In Secs. III and IV results for the current-voltage (I-V) characteristic are presented, and the friction coefficient is discussed. We confirm Bobbert's result that the friction becomes *independent* of the shunt resistance for McCumber parameters $\beta_c \equiv 2eI_cR^2C/\hbar$ much larger than one. He correctly recognized the excitation of spin waves[8] as the source of additional friction, but an explanation of the magnitude of the friction is missing in his paper (the energy balance argument he provides is independent of the vortex velocity). We study the interaction between vortices and spin waves more closely, and give a semiquantitative explanation for the near linearity of the I-V curve in the flux-flow range. Our findings explain why experimentally[6] ballistic vortex motion could only be observed in a narrow parameter region. This is discussed in more detail in Sec. V.

A final section deals with the "row-switching" phenomenon, which leads to hysteretic steps in the I-V curve. An earlier suggestion to explain it by an analogy to solitonic vortex motion in a long Josephson junction is found to be inadequate.

II. CALCULATION

We use the RCSJ (resistively capacitively shunted junction) model for a square lattice of Josephson junctions. Our variables are the charges $\{Q_i\}$, and the order parameter phases $\{\varphi_i\}$ (at some interior point $\mathbf{r}_i$) of the superconducting islands connected by the junctions. Their equations of motions are

$$\frac{d}{dt}\varphi_i = \frac{2e}{\hbar}U_i, \tag{1}$$

$$\frac{d}{dt}Q_i = -\sum_{\langle ji\rangle}[I_c \sin(\varphi_i - \varphi_j - A_{ij}) + (U_i - U_j)/R] + I_{\text{external}}. \tag{2}$$

Here the sum runs over islands j connected to island i by a junction. The current I_{external} equals the applied current I_a at one side of the array, $-I_a$ at the opposite side, and vanishes for the interior islands. Perpendicular to the external current direction we use periodic boundary conditions. A homogeneous external magnetic field per-

pendicular to the array plane causes frustration; it enters the equations of motion via the line integrals of its vector potential $\mathbf{A}$,

$$A_{ij} = (2e/c\hbar) \int_{\mathbf{r}_i}^{\mathbf{r}_j} \mathbf{A}(\mathbf{r}) \cdot d\mathbf{r}.$$

Magnetic fields created by the Josephson currents are neglected. This is justified for small lattice constants and low critical currents. The electrostatic potentials $\{U_i\}$ of the islands are related to the charges by

$$Q_i = \sum_{\langle ji \rangle} C(U_i - U_j). \tag{3}$$

The array geometry is shown in Fig. 1.

The calculation of the potentials for given charges must be done for each step in the numerical integration of the equations of motion (1), (2). Since the capacitance matrix is diagonal in Fourier space for a homogeneous array,[9] this can be significantly speeded up by solving for the U_i in Fourier space. For N islands in the array it takes only $\mathcal{O}(N \log N)$ operations using a fast Fourier transform, whereas N^2 operations are required to multiply the (long-ranged) inverse capacitance matrix in real space with the charge vector. This trick, in a somewhat different guise, was applied before by Eikmans and Van Himbergen.[10]

A single vortex can be accommodated in the system by choosing a frustration equal to the inverse number of dual lattice sites (for zero frustration the periodic boundary conditions would generate an additional antivortex). It is, however, not easy to construct, or guess, the phase configuration containing exactly one vortex in the middle of the array. Therefore we start with a random initial-phase configuration, which usually contains many vortices and antivortices. Monitoring the vorticity (see the Appendix for its precise definition) of all plaquettes, we let the system evolve until all vortex-antivortex pairs are annihilated, and just one vortex is left. By translating the phase configuration this vortex is positioned in the middle of the array; then the "measurement" of the I-V curve is started. After each change of the bias current the system is typically given a time $10RC$ to equilibrate.

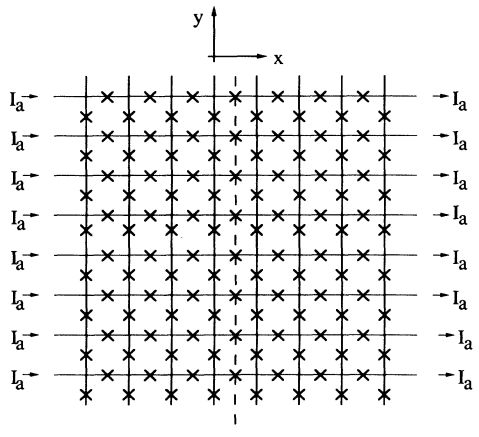

FIG. 1. The topology of the array used for the numeric calculations. The applied current I_a flows in the x direction, in the y direction periodic boundary conditions are used. The dashed line indicates the vortex path. In this array $N_x \times N_y = 7 \times 8$.

III. CURRENT-VOLTAGE CHARACTERISTIC

Figure 2 shows I-V curves of an array with $N_x \times N_y = 15 \times 32$ plaquettes for $\beta_c = 10$ and $\beta_c = 100$ (see Fig. 1 for the orientation of the coordinate system). The total dc voltage across the array in the I_a direction, divided by the number N_x of junctions in that direction, is V. The vortex depins at $I_a \approx 0.1 I_c$, in agreement with Ref. 1. Its average velocity v is given by

$$2\pi \frac{\hbar}{2e} \frac{v}{N_y a} = N_x V, \tag{4}$$

because each time a vortex moves through all N_y plaquettes in the y direction, the total phase difference across the array in the x direction changes by 2π, leading to an average voltage according to Eq. (1). After depinning, the vortex velocity rises roughly linearly with I_a for a large interval [cf. Fig. 2(b); note the scale difference as compared to Fig. 2(a)]. This region is called the flux-flow regime. At its upper end a small, staircase-like structure is seen for $\beta_c = 100$. It is caused by a phase locking between the vortex and spin waves it excited during its previous passage through the array. For a single vortex configuration, this phase locking is therefore related to our use of periodic boundary conditions in the y direction. For a larger array with the same β_c the structure disappears [see Fig. 2(c)]; we shall come back to this point below (cf. Fig. 7). In a real array there will of course be no periodic boundary conditions, and a vortex cannot reencounter spin waves it previously excited. However, if several vortices are present, we may expect that a vortex phase locks to the spin waves generated by a second vortex moving in front of it.

In the flux-flow regime, the phases only change in time when the vortex passes by, and come to rest in a time of order RC after the vortex has moved on. The rate of change of the phase difference across a junction, i.e., the voltage across it, increases with decreasing distance between the junction and the vortex core [see Fig. 3(a)]. Only the voltage across the junctions that are right in the vortex path has a dc component.

At $I_a \approx 0.78 I_c$ for $\beta_c = 10$, and $I_a \approx 0.6 I_c$ for $\beta_c = 100$, the flux-flow regime ends with a jump of the voltage. At this point the character of the phase motion is altered completely, and the phase motion is no longer dominated by the vortex. The row of junctions in the original vortex path, and one (for $\beta_c = 100$) or more (2 for $\beta_c = 10$) neighboring junction rows on either side transit to the nonzero voltage state. The voltage across each of these rows is now nearly exclusively dc, while the remaining junctions in the array show hardly any voltage across them [see Fig. 3(b)]. The total dc voltage across the array equals the number of rows that switched times the voltage across a single, current-biased junction in the nonzero voltage state.

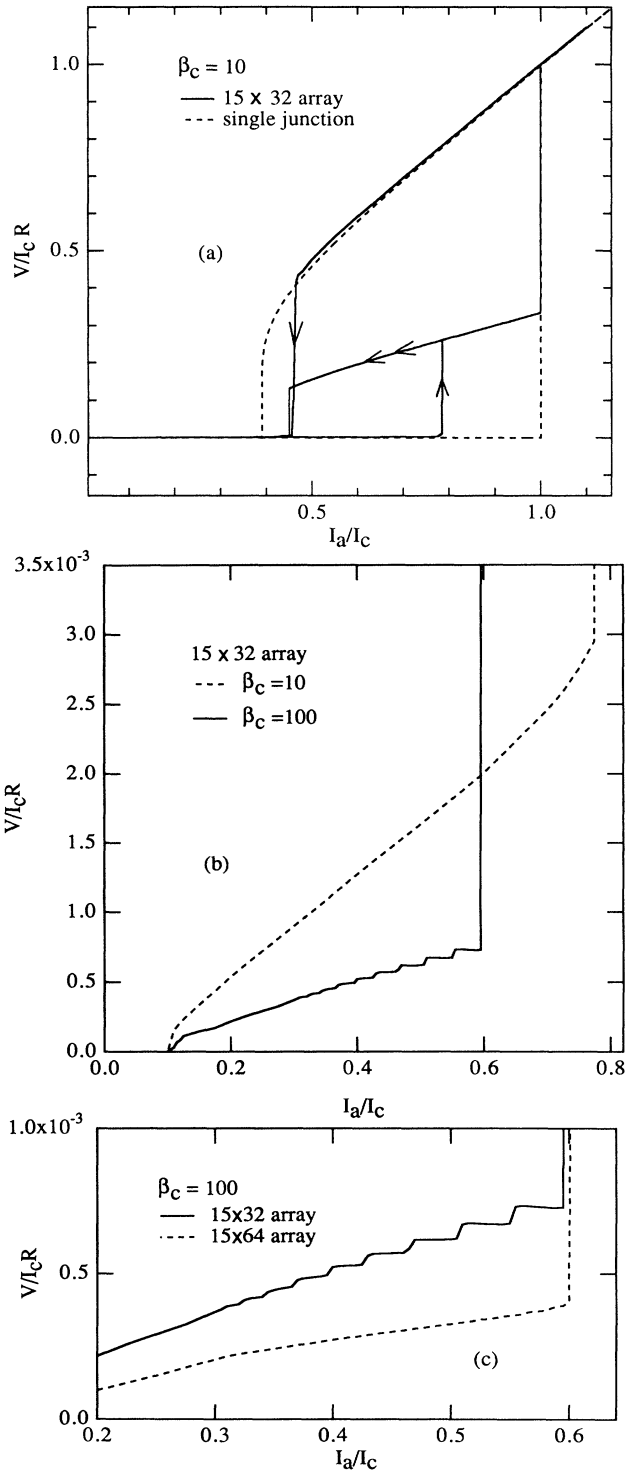

FIG. 2. *I-V* characteristic. (a) Full range. The branch indicated by the double arrow is followed if one reduces the current after the row switching occurred, but before reaching I_c. The single-junction behavior is shown here in dashed line for comparison. (b) Flux-flow regime. Notice the enlarged vertical scale as compared to (a). (c) Flux-flow regime for $\beta_c = 100$. Notice that the staircaselike structure is absent in the 15 × 64 array. In (b) and (c) the decreasing current branch is omitted.

The vortex topologically survives this row switching in the sense that the net number of vortices remains unity, but it loses its dynamical significance. It is now related to a time independent offset between the phase differences across neighboring junctions. Also, additional vortex-antivortex pairs are present constantly ($\beta_c = 100$) or appear and vanish periodically ($\beta_c = 10$). We shall return in Sec. VI to the question of what determines the current

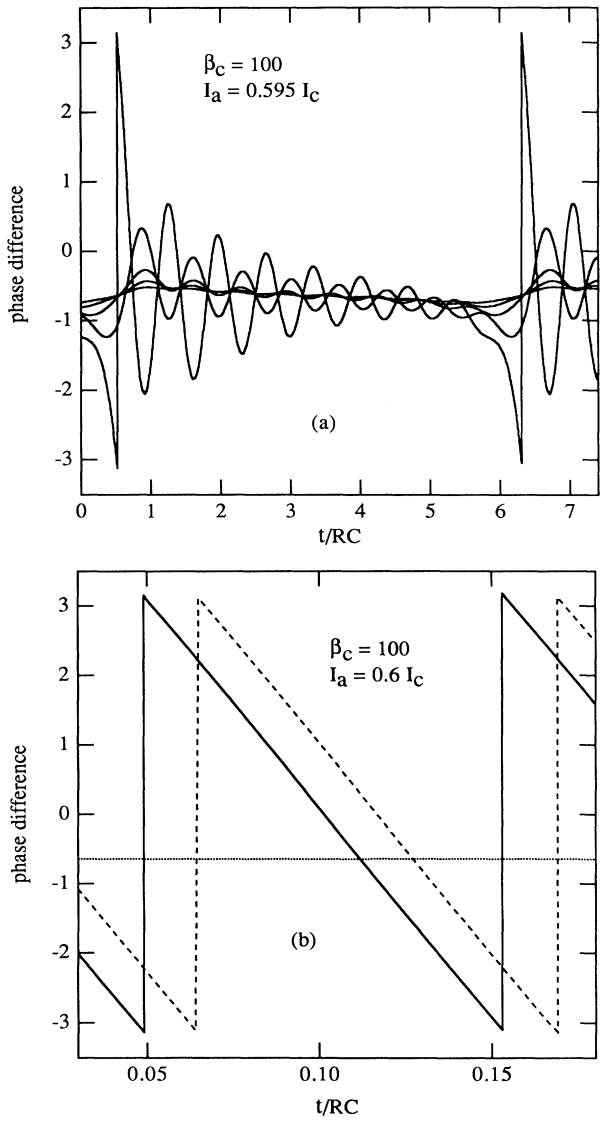

FIG. 3. Phase differences across junctions in the x direction vs time. The periodicity of the curves is due to the use of periodic boundary conditions in the y direction. (a) Before row switching. The curve with the largest amplitude corresponds to the central junction row (the one in the vortex path), the next largest to the neighboring row, etc. (b) After row switching. The solid line corresponds to the central junction row, and the dashed line to its two neighboring rows. All other phase differences in the x direction are given by the dotted line. Note the higher average vortex velocity as compared to (a).

value at which the row switching occurs.

For $I_a = I_c$, finally, all the remaining junctions in the x direction also switch to the nonzero voltage state, and the dc current flows through the shunting resistors. When the current is lowered again, the voltage stays close to RI_a also for I_a below I_c, reflecting the hysteresis of a single underdamped junction. In fact the I-V curve of the array nearly coincides here with that of a single junction [see Fig. 2(a)]. The retrapping current, however, is somewhat higher in the array.

When the junctions switch back to the zero-voltage state they may be in a configuration corresponding to additional vortex-antivortex pairs. Some of these do not leave the array immediately; this can cause small additional steps on the retrapping branch of the I-V curve. Also, the number of vortices and antivortices remaining in the array depends strongly on the rate at which I_a is decreased, and consequently so does the shape of the retrapping branch.

If one decreases the current after row switching occurred, but before $I_a = I_c$ is reached, there is also hysteresis. The retrapping current in this case is close to the retrapping current for the situation that I_a had been increased to above I_c [see Fig. 2(a)].

IV. FRICTION COEFFICIENT

In the flux-flow regime, for $I_a > 0.1I_c$ but below the row-switching current, the vortex velocity v is nearly linear in the applied current I_a, and one can define a friction coefficient η by equating the driving force exerted on the vortex by I_a (i.e., the energy supplied by the current source per unit length of the vortex path) to ηv,

$$\eta v \equiv \frac{2\pi}{a}\frac{\hbar}{2e}I_a = \frac{2\pi}{a}E_J\frac{I_a}{I_c}. \tag{5}$$

In the last member of this equation we introduced the Josephson energy E_J. For low McCumber parameters η is dominated by the resistors R shunting the junctions. In this case the value

$$\eta_0 = \left(\frac{\hbar}{2e}\right)^2\left(\frac{2\pi}{a}\right)^2\frac{1}{2R} \tag{6}$$

for η was derived in Refs. 4 and 5.

In Fig. 4 our numerical results for η are plotted versus $\sqrt{\beta_c}$. Clearly, the result (6) is quite good for β_c of order one. However, η/η_0 then rises roughly proportional to $\sqrt{\beta_c}$,

$$\eta \approx \eta_0\frac{\sqrt{\beta_c}}{\pi} = \left(\frac{\hbar}{2e}\right)^2\left(\frac{2\pi}{a}\right)^2\frac{1}{\pi}\sqrt{\frac{2eI_cC}{\hbar}} = \frac{2\pi}{a^2}\frac{E_J}{\omega_p} \tag{7}$$

in agreement with Bobbert's[7] findings. Note that this expression for the friction coefficient η depends only on E_J and the Josephson plasma frequency $\omega_p \equiv \sqrt{8E_Je^2/2C}/\hbar = \sqrt{\beta_c}/RC$, but it is *independent* of the resistance R — at first sight a surprising result. In terms of the vortex velocity it means that $v \approx a\omega_pI_a/I_c$ in the flux-flow regime for a strongly underdamped array.

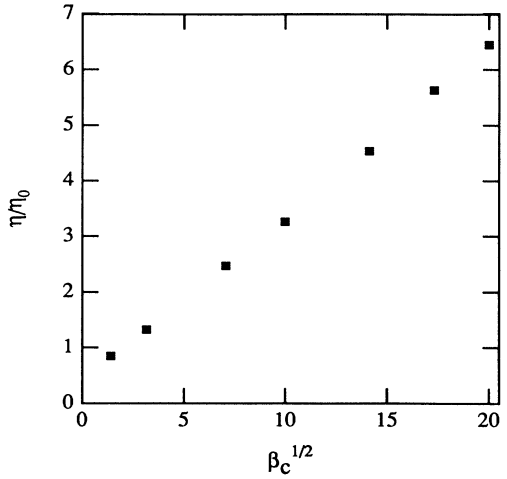

FIG. 4. The friction coefficient η, normalized by η_0, vs the square root of the McCumber parameter β_c. Here η is calculated at $I_a = 0.4I_c$.

Our simple explanation of the independence on R is that the vortex excites charge oscillations (or spin waves) on the islands adjacent to its path. These excitations do not propagate along with the vortex, which therefore loses energy by creating charge oscillations on each new island it passes. This mechanism for vortex friction was already speculated about in Ref. 11. The resistance R determines the decay time RC of the charge oscillations, but for $v > a/RC$ the vortex has moved on before the Ohmic damping becomes effective, and R does not influence the amount of energy transferred from the vortex to the charge oscillations.

While the independence of η on R is thus easy to understand, it is not clear why this damping mechanism should lead to a linear I-V curve, i.e., a velocity-proportional friction. In fact, we conclude that it does not: for high β_c the flux-flow branch is neither strictly linear nor does its extrapolation to $I_a = 0$ pass through the origin.

In order to gain some understanding of the shape of the I-V curve we first consider an infinite array in the continuum limit. In this limit the equation of motion (2) for the charge becomes linear,

$$\frac{\partial}{\partial t}Q(\mathbf{r},t) = I_c\nabla^2\varphi(\mathbf{r},t) + \frac{1}{R}\nabla^2U(\mathbf{r},t). \tag{8}$$

(We omitted the vector potential, which is not needed to accommodate a single vortex if no periodic boundary conditions are used.) The symbol Q now denotes the (areal) charge density, and ∇^2 is the Laplace operator. Combining (8) with the Josephson relation (1) and Poisson's equation

$$\nabla^2U = -Q/C, \tag{9}$$

the continuum limit of Eq. (3), we obtain for a nonsingular phase field

$$\frac{\partial^2}{\partial t^2}Q(\mathbf{r},t) + \omega_p^2Q(\mathbf{r},t) + \frac{1}{RC}\frac{\partial}{\partial t}Q(\mathbf{r},t) = 0. \tag{10}$$

The charges at different positions behave as uncoupled harmonic oscillators. For $R \to \infty$ their eigenfrequency is the Josephson plasma frequency ω_p. Due to the lack of spatial coupling the dispersion relation of spin waves is of the "optical" type, i.e., their eigenfrequency does not depend on the wave vector, and their group velocity vanishes. They can therefore not carry away energy. In particular, this implies that the coupling between vortex and spin waves will not give rise to a damping force for a small-amplitude oscillatory motion of the vortex.

The spin-wave spectrum acquires an "acoustic" branch if the conducting islands are given a nonzero capacitance to ground. Friction due to acoustic spin waves has been studied in Refs. 2 and 3. Here we treat the case of a purely optical spectrum.

In the continuum model a single, static vortex with its center at $\mathbf{r}_0 = (x_0, y_0)$ corresponds to the starlike phase configuration

$$\varphi^V(\mathbf{r}) = \mathrm{Im} \ln [x - x_0 + i(y - y_0)]. \tag{11}$$

For a vortex moving with velocity $\mathbf{v}$ we define the spin-wave part φ^S of the phase configuration by the difference between the translating configuration (11) and the solution φ of the equations of motion (8), (1),

$$\varphi(\mathbf{r}, t) \equiv \varphi^V(\mathbf{r} - \mathbf{v}t) + \varphi^S(\mathbf{r}, t). \tag{12}$$

The spin-wave part is nonsingular, and $\oint \nabla\varphi^S \cdot d\mathbf{r}$ vanishes for any closed loop. The vortex contribution, on the other hand, is singular at the core, and there its partial space and time derivatives do not commute. Since φ^V is the solution for a static vortex we have

$$\nabla^2 \varphi^V(\mathbf{r} - \mathbf{v}t) = 0. \tag{13}$$

For the charge density Q^V connected to a moving vortex, on the other hand, we find (putting $x_0 = y_0 = 0$, $v_x = 0$, $v_y = v$)

$$\begin{aligned} Q^V \equiv -C\nabla^2 U^V &\equiv -C\nabla^2 \frac{\hbar}{2e}\frac{\partial}{\partial t}\varphi^V(\mathbf{r} - \mathbf{v}t) \\ &= C\nabla^2 \frac{\hbar}{2e} v \frac{\partial}{\partial x} \ln \sqrt{x^2 + (y - vt)^2} \\ &= C\frac{\hbar}{2e} v \frac{\partial}{\partial x} 2\pi\delta(x)\delta(y - vt). \end{aligned} \tag{14}$$

The spin-wave part Q^S of the charge density is defined analogously by $Q^S \equiv -C\nabla^2 U_S \equiv -C\nabla^2(\hbar/2e)\partial\varphi^S/\partial t$. From Eqs. (8), (9), and (1) one obtains for its motion

$$\frac{\partial^2}{\partial t^2} Q^S + \omega_p^2 Q^S + \frac{1}{RC}\frac{\partial}{\partial t} Q^S = -\frac{\partial^2}{\partial t^2} Q^V - \frac{1}{RC}\frac{\partial}{\partial t} Q^V. \tag{15}$$

Equations (14) and (15) describe how the moving vortex excites spin waves.

We now calculate how much energy the vortex loses to the spin waves when it moves. The total energy E^S of the spin waves consists of the charging energy connected with Q^S and the (linearized) Josephson energy of the phase field φ^S,

$$E^S = \tfrac{1}{2}\int U^S Q^S d^2r + \tfrac{1}{2} E_J \int |\nabla\varphi^S|^2 d^2r. \tag{16}$$

Its rate of change is

$$\begin{aligned} \frac{\partial E^S}{\partial t} &= \int U^S \dot{Q}^S d^2r - E_J \int \dot{\varphi}^S \nabla^2 \varphi^S d^2r \\ &= \int U^S(\mathbf{r}, t) \left(\dot{Q}^S(\mathbf{r}, t) + \omega_p^2 \int^t Q^S(\mathbf{r}, t')dt' \right) d^2r \\ &= -\frac{1}{RC}\int U^S Q^S d^2r \\ &\quad + \int U^S \left(-\dot{Q}^V - \frac{1}{RC} Q^V \right) d^2r, \end{aligned} \tag{17}$$

where we have used Eq. (15) in the last step. The rate of change of the spin-wave energy consists of a loss term due to Ohmic friction, and the gain term

$$\left(\frac{\partial E^S}{\partial t}\right)^+ \equiv -\int U^S \left(\dot{Q}^V + \frac{1}{RC} Q^V \right) d^2r \tag{18}$$

due to coupling to the moving vortex. Evaluation of the gain term is more convenient after a spatial Fourier transform; using Eqs. (14) and (15) one finds

$$\left(\frac{\partial E^S}{\partial t}\right)^+ = \frac{v^3 E_J}{2\Omega\omega_p^2} \int d^2k \frac{k_x^2 k_y}{k_x^2 + k_y^2} [(vk_y)^2 + (RC)^{-2}] \left(\frac{(2RC)^{-1}}{(k_y v - \Omega)^2 + (2RC)^{-2}} - \frac{(2RC)^{-1}}{(k_y v + \Omega)^2 + (2RC)^{-2}} \right). \tag{19}$$

Here Ω is the eigenfrequency $\sqrt{\omega_p^2 - (2RC)^{-2}}$ of the damped charge oscillations. The integral in (19) diverges for large k. This stems from our use of a coreless vortex. In the array there is a natural cut-off at the wave vector π/a, which we shall therefore also impose on the integral in (19).

For $R \to \infty$, the strongly underdamped case we are most interested in, Eq. (19) then takes the form

$$\begin{aligned} \left(\frac{\partial E^S}{\partial t}\right)^+ &= \frac{v^3 E_J}{2\omega_p^3} \int_{-\pi/a}^{\pi/a} dk_x \int_{-\pi/a}^{\pi/a} dk_y \frac{k_x^2 v^2 k_y^3}{k_x^2 + k_y^2} \pi [\delta(\omega_p - k_y v) - \delta(\omega_p + k_y v)] \\ &= (2\pi E_J v/a)\Theta(v - a\omega_p/\pi)\pi \left(1 - \frac{\arctan(\pi v/a\omega_p)}{\pi v/a\omega_p} \right). \end{aligned} \tag{20}$$

A formula for the vortex velocity can now be obtained by equating $(\partial E^S/\partial t)^+$ to the energy transferred per unit time to the vortex by the external current,

$$\Theta(v - a\omega_p/\pi)\pi\left(1 - \frac{\arctan(\pi v/a\omega_p)}{\pi v/a\omega_p}\right) = \frac{I_a}{I_c}. \quad (21)$$

According to formula (20) there is no frictional force on the vortex for $v < a\omega_p/\pi$. This is related to the sharp wave-vector cut-off employed. Introducing instead the smooth cut-off function $\exp(-ka/\sqrt{2\pi})$ (used in Ref. 3) in the integrand in Eq. (19) we obtain

$$\frac{a\omega_p}{v}\int_0^\infty d\xi \frac{\xi^2}{1+\xi^2}\exp\left(-\sqrt{\frac{\xi^2+1}{2\pi}}\frac{a\omega_p}{v}\right) = \frac{I_a}{I_c}. \quad (22)$$

Figure 5 shows the vortex velocity versus the applied current according to both Eqs. (21) and (22), together with results of the numerical calculation. [The Heaviside function of Eq. (21) is omitted in that figure.] We observe that the continuum model gives the right order of magnitude, although it overestimates the friction by about a factor of 2. Also, of course, pinning by the lattice-periodic Josephson potential, which for the array inhibits vortex motion for I_a lower than about $0.1I_c$, is absent in the continuum model. A very important feature of the energy loss to spin waves is that it strongly decreases for a vortex velocity very small compared to $a\omega_p$. Unfortunately, in the region of low velocity the results of the continuum model depend on details of the cut-off; the model therefore only provides us with a rough indication of the velocity range in which spin-wave friction can be neglected.

The continuum model has been studied before by Eckern and Schmid.[3] These authors disregarded the vortex friction due to the excitation of optical spin waves because they focused on the limit $v/a\omega_p \to 0$. However, if one is interested in modeling ballistic vortex motion in the array for $I_a = 0$, the velocity of the vortex cannot be arbitrarily low, because the vortex kinetic energy at the bottom of the pinning potential must not be smaller than the amplitude of the pinning potential, about $0.2E_J$ for the square lattice. Using the result

$$m = \left(\frac{\hbar}{2e}\right)^2\left(\frac{2\pi}{a}\right)^2\frac{C}{2}, \quad (23)$$

from Refs. 2–5 for the vortex mass this implies that the vortex velocity must reach at least $a\omega_p\sqrt{0.2}/\pi \approx 0.15a\omega_p$ whenever the vortex moves by a lattice constant. According to Eq. (22) the friction due to the excitation of optical spin waves is already effective at this velocity (see also Fig. 5).

In the "linear medium approximation" also studied in Ref. 3 the pinning potential is taken into account, so that in that model the limit of vanishing vortex velocity is not an option. The reason why the friction mechanism discussed in this paper was not noticed for the linear medium approximation of Ref. 3 is not entirely clear.

We shall now examine the results of the numerical calculation in light of the above discussion. In Fig. 6 we plot $\omega_p^2 Q_i$ as a function of time for an island i next to the vortex path, together with

$$\omega_p^2 Q_i^{V,\text{eff}} \equiv \ddot{Q}_i + \omega_p^2 Q_i + \frac{1}{RC}\dot{Q}_i. \quad (24)$$

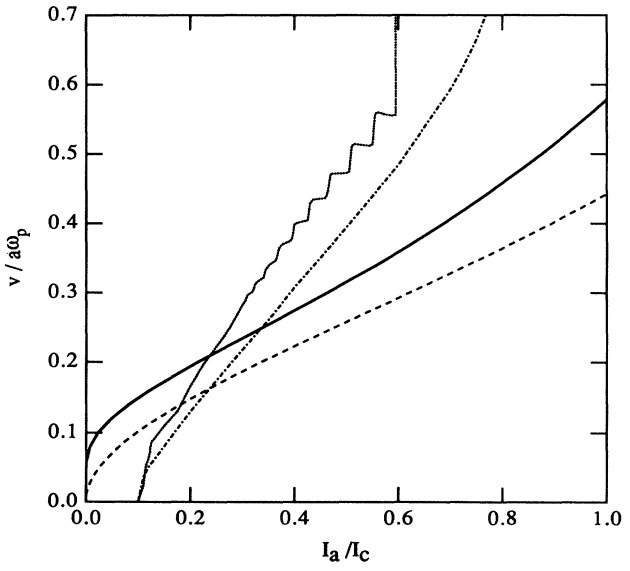

FIG. 5. Vortex velocity vs applied current according to the continuum model with sharp cut-off [dashed line, cf. Eq. (21), with the Heaviside function omitted] and exponential cut-off [solid line, cf. Eq. (22)] at $\beta_c = \infty$. Also shown are numerical results for the 15×32 array at $\beta_c = 10$ (dashed-dotted line) and at $\beta_c = 100$ (dotted line).

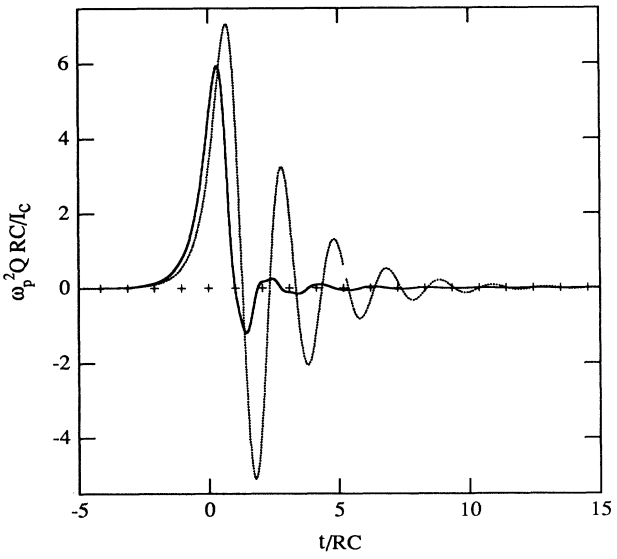

FIG. 6. Solid line: effective charge [cf. Eq. (24)] on an island next to the vortex path. Dotted line: total charge on the same island. Crosses + indicate times at which the vortex passes a junction.

This quantity is the effective charge connected with the moving vortex if one enforces Eq. (15). Also shown in Fig. 6 is the position of the vortex. At $t = 0$ the vortex enters the plaquette bounded by the island i under consideration. We see that $Q_i^{V,\text{eff}}$ is essentially different from zero only if the vortex is less than about two lattice constants away. The charge oscillations created by $Q_i^{V,\text{eff}}$ decay like $\exp(-t/2RC)$, and persist for some time after the vortex has moved on. This can also be seen in Figs. 7(a) and 7(b), which show "snapshots" of the charge distribution. Appreciable charge oscillations occur only on two island rows in the wake of the vortex. For the parameters $I_a = 0.5I_c$ and $\beta_c = 100$ used in Fig. 7, the charge oscillations have not yet died out completely in the time it takes the vortex to travel 32 lattice constants. This causes the staircaselike feature in the I-V curve of the 15×32 array, which is absent in the 15×64 array for the same β_c [cf. Figs. 2(c) and 7].

The time integral of $\omega_p^2 Q_i^{V,\text{eff}}$ equals $\pm 2\pi I_c$ for an island next to the vortex path and vanishes elsewhere. To understand this fact note that (for an infinite array)

$$\begin{aligned}\int_{-\infty}^{\infty} \omega_p^2 Q_i^{V,\text{eff}} dt &= \int_{-\infty}^{\infty} \left(\ddot{Q}_i + \omega_p^2 Q_i + \frac{1}{RC}\dot{Q}_i \right) dt \\ &= \omega_p^2 \int_{-\infty}^{\infty} Q_i dt \\ &= \omega_p^2 \int_{-\infty}^{\infty} \sum_{\langle ji \rangle} C(U_i - U_j) dt \\ &= I_c \sum_{\langle ji \rangle} (\varphi_i - \varphi_j)|_{-\infty}^{\infty}. \end{aligned} \tag{25}$$

The sum over phases in this equation equals $\pm 2\pi$ or 0, as can be seen from the sketch in Fig. 8. While the

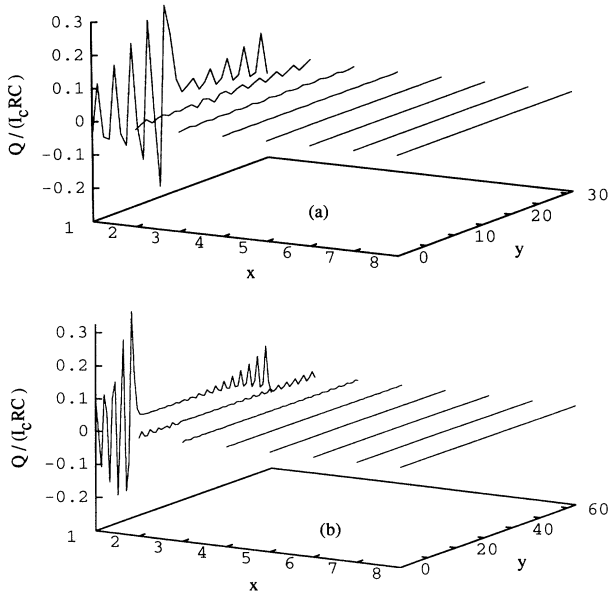

FIG. 7. Snapshots of the charge distribution in a 15×32 array (a) and a 15×64 array (b), for $I_a = 0.5I_c$ and $\beta_c = 100$. In the x direction we show only half of the array for clarity.

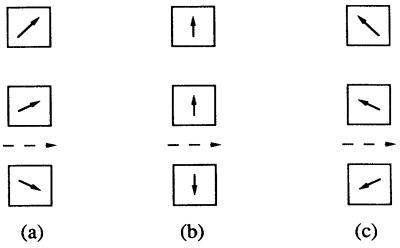

FIG. 8. Sketch of the phases on islands next to the vortex path before the vortex passes (a), at the passage of the vortex (b), and after passage of the vortex (c). Dashed line indicates vortex path. Notice that phase differences across the vortex path increases by 2π, while other phase difference have zero net change.

complete time integral of $\omega_p^2 Q^{V,\text{eff}}$ is a constant, the shape of the $Q^{V,\text{eff}}$ pulse depends somewhat on vortex velocity and McCumber parameter. Figure 9 displays $\int_{-\infty}^{t=x/v} dt' \omega_p^2 Q^{V,\text{eff}}(t')/(2\pi I_c)$ for various values of I_a and β_c. The differences between the curves appear minor for I_a not too close to the value at which row switching sets in. Except for the dip at $x \approx -a$ they also agree quite well with what one would expect from a star-shaped phase configuration for the vortex from the continuum model [cf. Eq. (11)]

$$\begin{aligned}&\int_{-\infty}^{t=x/v} dt' \omega_p^2 Q^{V,\text{star}}(t')/I_c \\ &\equiv 4\,\text{Im}\ln\left(\frac{1}{2} - i\frac{vt}{a}\right) \\ &\quad - \sum_{l=\pm 1} \left\{ \text{Im}\ln\left(\frac{1}{2} + l - i\frac{vt}{a}\right) \right. \\ &\quad \left. + \text{Im}\ln\left[\frac{1}{2} - i\left(\frac{vt}{a} + l\right)\right] \right\}. \end{aligned} \tag{26}$$

Close to the current where row switching happens, the oscillations excited by the passing vortex develop such a large amplitude that the linearization of the Josephson current for the spin waves fails. Then the right-hand side (RHS) of Eq. (24) is not only nonzero due to the vortex, but due to spin-wave anharmonicity as well (see the curve for $\beta_c = 10$ and $I_x = 0.78I_a$ in Fig. 9). Also, in that case charge oscillations on different islands become coupled, and the simple description of the charge oscillations in terms of independent harmonic oscillators breaks down completely. Row switching occurs in this regime.

V. VORTEX MASS AND INERTIA

As long as there is a linear relation between the vortex velocity and the applied current, the total charging energy of the array is quadratic in the vortex velocity. This follows from the fact that the energy supplied by the current source is ultimately converted into heat in the shunt resistors. For steady motion

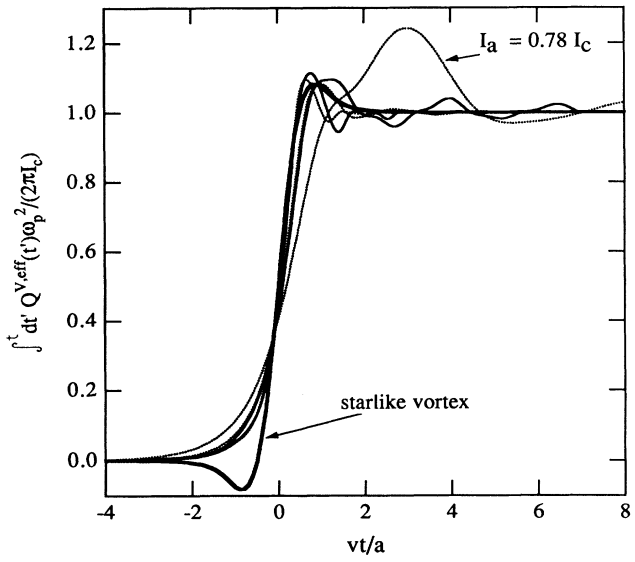

FIG. 9. The integral of the effective vortex charge vs vortex position. For $\beta_c = 10$ (dotted lines) curves corresponding to $I_a = 0.2, 0.4$, and 0.78 are shown, for $\beta_c = 100$ (thin full lines) curves corresponding to $I_a = 0.2$ and 0.4. The thick full line gives the result for a starlike vortex configuration [cf. Eq. (26)]. Note that as long as the current is not too close to the point where row switching occurs ($I_a = 0.78$ for $\beta_c = 10$), the curves fall close together.

$$\sum_{\langle ij \rangle} \frac{1}{R}(U_i - U_j)^2 = (N_y I_a)(N_x V) = 2\pi E_J \frac{v}{a}\frac{I_a}{I_c} \qquad (27)$$

thus holds. The left-hand side (LHS) equals the total charging energy divided by $RC/2$, and the RHS is quadratic in v for a linear I-V characteristic.

In the flux-flow regime the I-V curve turns out to be nearly linear, and consequently there the total charging energy is nearly quadratic in the vortex velocity, as must be required of the kinetic energy. Nevertheless only that part of the charging energy that travels along with the vortex qualifies as vortex kinetic energy; the remaining part is contained in the spin waves created by the vortex. Only in the adiabatic limit $v/a\omega_p \to 0$, when excitation of spin waves is suppressed, the total charging energy may be regarded as vortex kinetic energy. By considering this limit the expression (23) for the vortex mass m was derived in Refs. 2–5.

As already noted above, the adiabatic limit is only marginally realizable due to the lattice periodic pinning potential. If one approaches this limit, the vortex velocity will vary considerably over a lattice constant, an effect neglected in the derivations of m in Refs. 4 and 5. In the linear medium approximation developed in Ref. 3 the effect is accounted for, but found to have little effect on the vortex mass. One must keep in mind, of course, that the vortex position, and with it the vortex velocity, is not unambiguously defined within one plaquette. This ambiguity also affects the definition of the vortex mass.

Experimentally, Van der Zant *et al.*[6] found vortices moving ballistically over a distance of 60 lattice constants with a speed of about 2×10^9 lattice constants per second. Since $\omega_p = 1.2 \times 10^{11}\ s^{-1}$ in that experiment, the average vortex velocity was only about $0.016a\omega_p$. Due to the periodic pinning potential the peak velocity must have been higher, as discussed above. For the triangular lattice used in Ref. 6 the pinning barrier is about $0.05E_J$;[1] with the expression (23) this requires a peak velocity of $\sqrt{0.1E_J/m} = 0.07a\omega_p$. The results obtained in this paper suggest that these velocities might just be low enough to avoid the friction due to the excitation of optical spin waves (cf. Fig. 5). In this respect we disagree with Bobbert,[7] who inferred from the enhanced friction coefficient at vortex velocities not very small compared to $a\omega_p$ that ballistic vortex motion is impossible. However, we conclude that in the parameter region where ballistic motion can be achieved the pinning potential is never small compared to the vortex kinetic energy.

We also note that the McCumber parameter in Ref. 6 must have been extremely large. Since all charging energy decays exponentially with time constant RC, the observed path length of 60 lattice constants and the average vortex velocity of $0.016a\omega_p$ implies $0.016\omega_p RC > 60$, i.e., a McCumber parameter $\beta_c > 10^7$. The McCumber parameter calculated with the normal state tunnel resistance in Ref. 6 had the value 46. In that experiment there were no Ohmic shunts, but R is to model the subgap resistance for quasiparticle tunneling. The subgap resistance must thus have been $\sqrt{10^7/46} \approx 500$ times larger that the normal state tunnel resistance, which for high-quality tunnel junctions is not unreasonable.

In Ref. 6 the external current was applied in the left vertical part of an H-shaped array. The ballistic vortex moved through the channel (the "-" of the "H") and the right vertical part, where no external current was applied. Ballistic vortex motion could only be observed for very low currents just barely sufficient to depin the vortices. In the first instance one might expect that a higher current, resulting in a higher initial vortex velocity in the current-free part of the array, would do no harm, with the vortex just slowing down until friction by spin-wave excitations becomes ineffective. The reverse side of friction, however, is fluctuations, and charge oscillations created by a moving vortex can have a strong back-action on it after the driving current has been removed.

Figure 10 shows our numerical results for the motion of a vortex in a 15×64 array with $\beta_c = 2500$. At $t = 0$ the current I_a is reduced linearly from $0.15I_c$ to zero in a time $2\pi/\omega_p \approx 0.125RC$. We see that the vortex does not persist in its motion, but rather oscillates back and forth a couple of times. This one might interpret as the influence of a "fluctuating force" exerted on the vortex by the spin waves it created. It is possible that this effect spoiled ballistic vortex motion in Ref. 6 for higher initial vortex velocities.

To gain complete confidence in the interpretation of the Van der Zant-Orlando-Mooij experiment[6] in terms of ballistic vortex motion it is desirable to perform a computer simulation of the H-shaped array with extreme values of β_c. The computational requirements for such work are beyond the power of the work station on which the

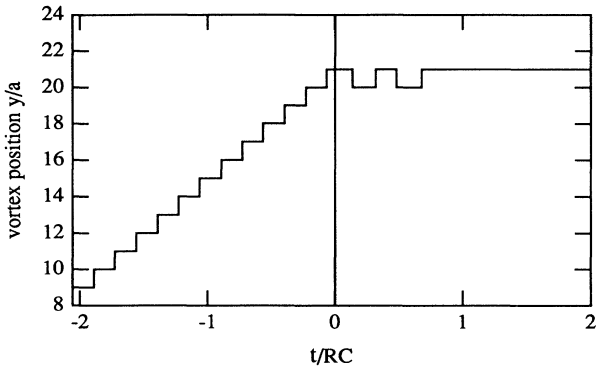

FIG. 10. Vortex motion at $\beta_c = 2500$ in the 15×64 array. The applied current is $0.15 I_c$ for $t < 0$, and is linearly decreased to zero between $t = 0$ and $t = 0.125$.

calculations reported in this paper were performed. An implementation on a faster machine is in progress.[12]

We conclude this section by a remark on the vortex mass in the quantum regime. If, by lowering capacitance and temperature, the unit charging energy $e^2/2C$ becomes small compared to the thermal energy, quantum fluctuations of the phases are important. A vortex can then behave as a quantum mechanical particle. Since it moves in the periodic pinning potential, its energy eigenvalues form a band structure. The band mass of the vortex has been calculated numerically for very small arrays,[13] and in the limit of high $E_J/(e^2/2C)$ analytically with an instanton method.[14,15] It was found to lie at least a factor 5 higher than the band mass obtained from a model Hamiltonian for vortex motion combining the free mass (23) with a sinusoidal pinning potential.[3] The enhancement of the band mass is also a consequence of the coupling between vortex and spin waves, which hinders vortex tunneling, thus making the band flatter and the band mass larger. However, as we have seen in Sec. IV, for translational motion of a classical vortex the coupling to the spin waves leads to additional friction rather than to an enhancement of the vortex inertia: the notion of vortex mass thus has a different meaning in different contexts.

VI. ROW SWITCHING

We finally return to the row-switching phenomenon. This instability of the vortex solution above a threshold current had already been predicted by Nakajima and Sawada[16] and was experimentally observed by Van der Zant *et al.*[17]

In Ref. 11 it is suggested that there exists an analogy between the vortex velocity at which row switching occurs and the maximum velocity of a soliton in a long Josephson junction. Such a soliton solution does not depend on space and time separately, but rather on the combination[18]

$$\left(\frac{y - vt}{\lambda_J}\right)\left(1 - \left(\frac{v}{\bar{c}}\right)^2\right)^{-\frac{1}{2}}. \tag{28}$$

Here λ_J is the Josephson-penetration depth and v the soliton velocity, which cannot exceed the limiting velocity $\bar{c} \equiv \omega_p \lambda_J$. We believe that this maximum soliton velocity bears little relation to the maximum vortex velocity in the arrays we studied.

First, λ_J is infinite in our system, since we neglected any magnetic field created by the Josephson currents. Furthermore, we see from Fig. 9 that the vortex does not suffer the Lorentz-like contraction characteristic for the soliton [the square-root denominator in Eq. (28)]. Finally, the velocity at which row switching occurs, measured in units of $a\omega_p$, decreases with increasing β_c, noted experimentally[11] as well as in the numerical work (cf. Ref. 7 and Fig. 2). This also differs from the behavior of the soliton in a long Josephson junction.

Qualitatively it is easy to understand what happens in the row switching. The individual underdamped Josephson junctions have a hysteretic I-V curve and are on the metastable part of the zero-voltage branch when the row switching occurs. External perturbations (e.g., noise) initiate the transition to the nonzero voltage branch for bias currents smaller than I_c. In our case the disturbance is provided by the passing vortex. In the discussion of Fig. 9 we already pointed out that for a I_a just below the row-switching value, large amplitude oscillations of the phases are created on islands the vortex passes. If the damping due to the shunt resistors is lowered, i.e., β_c increased, the metastable zero-voltage branch becomes more vulnerable to this disturbance.

A quantitative theory of the current value at which row switching sets in is not available at present. Some additional insight, however, can be gained by studying the related phenomenon in fully frustrated arrays,[19] for which a reduced description in terms of only 2 degrees of freedom is possible.

VII. SUMMARY

We have simulated square-lattice arrays of underdamped ($\beta_c > 1$) Josephson junctions containing one vortex by solving the full set of RCSJ equations for the coupled junctions. At moderate values of β_c, our simulations agree with a simple description of the vortices which assigns a mass (23) and a simple viscous damping parameter (6) to the vortex.

As Bobbert[7] has pointed out previously, however, this description breaks down for much higher values of β_c. An extra damping mechanism appears, so that even in the limit of arbitrarily small Ohmic loss in each junction, there will be a nonzero drag force on the vortex, see Eq. (7). We have discussed the physical origin of these extra losses in terms of the generation of charge oscillations by the moving vortex, and have developed an analytic theoretical description of the extra losses.

As a consequence of our analysis, we conclude that ballistic vortex motion should only be observed under very limited circumstances. Extremely high values of β_c, a driving current only slightly above the vortex depinning current, and arrays with weak pinning potential, such as triangular-lattice arrays, appear to be necessary to observe ballistic vortex motion. These are precisely the

conditions reported in the experimental work of Van der Zant *et al.*[6]

Note added in proof. Reference 20 contains experimental verification of the enhanced viscosity, Eq. (7), as well as a semiquantitative model to explain the enhancement.

ACKNOWLEDGMENTS

U.G. gratefully acknowledges financial support by the NATO Scientific Affairs Division via the DAAD. C.J.L. and C.B.W. received partial support from AFOSR Grant No. F49620-92-J-0041. We benefited from discussions with H. van der Zant, P. Bobbert, and M. Octavio.

APPENDIX: DEFINING VORTICITY IN A JOSEPHSON ARRAY

In a bulk superconductor, the net number n of vortices enclosed by a curve C is given by

$$n = \frac{1}{2\pi} \oint_C \nabla\varphi \cdot d\mathbf{l}. \tag{A1}$$

For $n \neq 0$ the phase field is multivalued, but $\nabla\varphi$ is (locally) well defined and unique. In applying (A1) to a junction array, however, an ambiguity arises, since the phase is not defined inside the tunnel barriers, and consequently phase differences across the junctions are only determined up to a multiple of 2π. To get a definite result, one needs to establish an additional rule on how to choose this multiple.

It is natural to restrict the value of the phase difference across a tunnel barrier to the range $-\pi$ to π, i.e., to use the value of the phase difference with minimum modulus. If the phases are uniform inside each superconducting island, the vorticity of a plaquette is then defined by

$$n = \frac{1}{2\pi} \sum_i \left[\varphi_{N(i)} - \varphi_i\right]_{mmr}, \tag{A2}$$

where i runs over all superconducting islands forming the plaquette, $N(i)$ is the neighbor of i in counterclockwise direction, and $[\varphi]_{mmr}$ indicates the application of the above "minimum-modulus-rule" to φ. This rule is essential [without it, Eq. (A2) would always give $n = 0$!] and implicitly used, though not spelled out, in much of the literature.

If an external magnetic field with vector potential $\mathbf{A}$ is present, the phases on the islands are no longer constant. Inside the islands, the supercurrent density is usually so low that in good approximation

$$\nabla\varphi = -\frac{2e}{\hbar c}\mathbf{A} \tag{A3}$$

holds. In this case the array analogue of (A1) becomes

$$\begin{aligned} n &= \frac{1}{2\pi} \int_{\text{inside islands}} \nabla\varphi \cdot d\mathbf{l} + \frac{1}{2\pi} \sum_i \left[\varphi_{N(i)} - \varphi_i - \frac{2e}{\hbar c} \int_{\mathbf{r}_{N(i)}}^{\mathbf{r}_i} \mathbf{A} \cdot d\mathbf{l}\right]_{mmr} \\ &= -\frac{2e}{hc} \oint \mathbf{A} \cdot d\mathbf{l} + \frac{1}{2\pi} \sum_i \left[\varphi_{N(i)} - \varphi_i - \frac{2e}{\hbar c} \int_{\mathbf{r}_{N(i)}}^{\mathbf{r}_i} \mathbf{A} \cdot d\mathbf{l}\right]_{mmr}. \end{aligned} \tag{A4}$$

Here $\mathbf{r}_i$ is some point inside island i and φ_i the phase at the point. The first term in the last member of this equation is (up to the sign) the frustration, i.e., the flux through the plaquette normalized by the flux quantum. The second term sums the gauge-invariant phase differences (with the minimum-modulus-rule applied). The latter just expresses the phase differences across the tunnel barriers in terms of the phases φ_i in the interior of the islands. They also occur in the Josephson currents [cf. Eq. (2)].

[1] C.J. Lobb, D.W. Abraham, and M. Tinkham, Phys. Rev. B **27**, 150 (1983).
[2] A.I. Larkin, Yu. N. Ovchinnikov, and A. Schmid, Physica **152B**, 266 (1988).
[3] U. Eckern and A. Schmid, Phys. Rev. B **39**, 6441 (1989).
[4] M. Rzchowski, S. Benz, M. Tinkham, and C.J. Lobb, Phys. Rev. B **42**, 2041 (1990).
[5] T.P. Orlando, J.E. Mooij, and H.S.J. van der Zant, Phys. Rev. B **43**, 10218 (1991).
[6] H. Van der Zant, Doctoral thesis, Technical University, Delft, 1991 (unpublished); H.S.J. van der Zant, F.C. Fritschy, T.P. Orlando, and J.E. Mooij, Europhys. Lett. **18**, 343 (1992).
[7] P.A. Bobbert, Phys. Rev. B **45**, 7540 (1992).
[8] Following the literature, we here call "spin waves" the small-amplitude oscillations of the order parameter phases, that do not change the vorticity.
[9] The application of the FFT requires periodic boundary conditions. In the direction of the applied current we therefore enlarge the array by its mirror image for the calculation of the voltages.
[10] H. Eikmans and J.E. van Himbergen, Phys. Rev. B **41**, 8927 (1990).
[11] H.S.J. van der Zant, F.C. Fritschy, T.P. Orlando, and J.E. Mooij, Phys. Rev. Lett. **66**, 2531 (1991).
[12] H. La Roche (private communication).
[13] U. Geigenmüller and G. Schön, Physica **165&166B**, 941 (1990).
[14] U. Geigenmüller, in *Macroscopic Quantum Phenomena*, edited by T.D. Clark *et al.* (World Scientific, Singapore, 1991).
[15] R. Fazio, U. Geigenmüller, and G. Schön, in *Quantum Fluc-*

tuations in Mesoscopic and Macroscopic Systems, edited by H.A. Cerdeira *et al.* (World Scientific, Singapore, 1991).
[16]K. Nakajima and Y. Sawada, J. Appl. Phys. **52**, 5732 (1981).
[17]H.S.J. van der Zant, C.J. Muller, L.J. Geerligs, C.J.P.M. Harmans, and J.E. Mooij, Phys. Rev. B **38**, 5154 (1988).
[18]A. Barone and G. Paterno, *Physics and Applications of the Josephson Effect* (Wiley-Interscience, New York, 1982).
[19]M. Octavio, C.B. Whan, U. Geigenmüller, and C.J. Lobb, Phys. Rev. B (to be published).
[20]H.S.J. van der Zant, F.C. Fritschy, T.P. Orlando, and J.E. Mooij, Phys. Rev. B **47**, 295 (1993).